Cell. Mol. Life Sci. (2012) 69:993–1009
DOI 10.1007/s00018-011-0826-z

Cellular and Molecular Life Sciences

RESEARCH ARTICLE

Modelling a ciliopathy: Ahi1 knockdown in model systems reveals an essential role in brain, retinal, and renal development

Roslyn J. Simms · Ann Marie Hynes · Lorraine Eley · David Inglis · Bill Chaudhry · Helen R. Dawe · John A. Sayer

Received: 9 March 2011 / Revised: 9 September 2011 / Accepted: 12 September 2011 / Published online: 29 September 2011

Abstract Joubert syndrome and related diseases (JSRD) are cerebello-oculo-renal syndromes with phenotypes including cerebellar hypoplasia, retinal dystrophy, and nephronophthisis (a cystic kidney disease). Mutations in *AHI1* are the most common genetic cause of JSRD, with developmental hindbrain anomalies and retinal degeneration being prominent features. We demonstrate that Ahi1, a WD40 domain-containing protein, is highly conserved throughout evolution and its expression associates with ciliated organisms. In zebrafish *ahi1* morphants, the phenotypic spectrum of JSRD is modeled, with embryos showing brain, eye, and ear abnormalities, together with renal cysts and cloacal dilatation. Following *ahi1* knockdown in zebrafish, we demonstrate loss of cilia at Kupffer's vesicle and subsequently defects in cardiac left–right asymmetry. Finally, using siRNA in renal epithelial cells we demonstrate a role for Ahi1 in both ciliogenesis and cell–cell junction formation. These data support a role for Ahi1 in epithelial cell organization and ciliary formation and explain the ciliopathy phenotype of *AHI1* mutations in man.

Keywords Cilia · Genetics · Zebrafish · Joubert syndrome · Cystic kidney disease · Retina · Development · Kupffer's vesicle · Left–right asymmetry · Epithelial cell

Electronic supplementary material The online version of this article (doi:10.1007/s00018-011-0826-z) contains supplementary material, which is available to authorized users.

R. J. Simms · A. M. Hynes · L. Eley · B. Chaudhry · J. A. Sayer (✉)
Institute of Genetic Medicine, Newcastle University, Central Parkway, Newcastle upon Tyne NE1 3BZ, UK
e-mail: j.a.sayer@ncl.ac.uk

D. Inglis
Sir William Dunn School of Pathology, University of Oxford, South Parks Road, Oxford OX1 3RE, UK

H. R. Dawe
Biosciences: College of Life and Environmental Sciences, University of Exeter, Stocker Road, Exeter EX4 4QD, UK

Introduction

Joubert syndrome and related diseases (JSRD) are autosomal recessive disorders, characterized by a developmental mid-hindbrain malformation. "Molar tooth sign" is the pathognomonic feature on cerebral MRI, which defines the cerebellar vermis hypoplasia, abnormally deep interpeduncular fossa, and elongated superior cerebellar peduncles diagnostic of Joubert syndrome (JBTS) [1]. Consequently, neurological anomalies can include hypotonia, ataxia, gaze palsy including oculomotor apraxia, learning difficulties, and abnormal neonatal breathing patterns. JSRD is considered a multisystem disease, with extra-neurological features including retinal degeneration [1–3], coloboma, cystic kidney disease (nephronophthisis [4] and multicystic renal dysplasia [5]), polydactyly and hepatic fibrosis [6, 7].

In addition to the clinical heterogeneity of JSRD, 11 causal genes have been identified in patients. These include JBTS types 1-11: *INPP5E* [8], *TMEM216* [9], *AHI1* [4, 9], *NPHP1* [11], *CEP290* [12–14], *TMEM67* [15, 16], *RPGRIP1L* [5], *ARL13B* [17], *CC2D2A* [18], *CXORF5* [19] and *TCTN2* [22]. The protein products encoded by all of these genes have been localized in the primary cilium [20], a highly conserved cellular organelle, central to the regulation of cellular signaling pathways [21]. *TCTN2* is a gene that has recently been associated with JBTS in three families [22]. Defects in ciliogenesis were observed follow *Tctn2* knockdown in vivo [22]. Acknowledgment of the fact that the protein products of all of these genes have a role in the primary cilium, explains why JBTS, nephronophthisis, and other disorders caused by mutations in these genes are referred to as ciliopathies [21].

Mutations in *AHI1* (Abelson-helper integration site-1) are a common genetic cause of JBTS, accounting for 12% of cases, and 20% of individuals with JBTS and Leber's congenital amaurosis [9, 23–26]. *AHI1* is highly conserved throughout evolution and encodes the Ahi1 protein (also known as Jouberin) [9]. By performing a detailed in silico search of proteomes of eukaryotic organisms, we have now identified additional homologues, confirming a conserved role for this gene between ciliated protozoa and man.

We have previously demonstrated that Ahi1 localizes to centrosomes/basal bodies of renal epithelial cells, and that it interacts with the protein product of *NPHP1*, nephrocystin-1 [27]. At a genomic level, there is evidence for *AHI1* mutations or polymorphisms having an oligogenic affect and modulating the phenotype. Five patients with homozygous *NPHP1* mutations combined with a R830W mutation in *AHI1* have been identified [28]. This triallelism resulted in a more severe CNS defect [28]. Similarly, the relative risk (RR) of a retinal defect (such as retinal dystrophy) associated with nephronophthisis was significantly increased (RR = 7.5; 95% CI 4.0–11.2) in the presence of the R830W *AHI1* mutation [26]. Early expression (from embryonic day 10.5) of Ahi1 is seen in murine brain, which persists into adulthood [9]. Previous work using zebrafish embryos aged 2.5–5 days post-fertilization has documented an expression pattern for *ahi1* in the brain (olfactory bulb, telencephalon, diencephalon, tectum, and cerebellum) and retina [29].

Given this evidence implicating an important role for *AHI1* in modulating brain, eye, and other phenotypes in JSRD, we investigated the effect of *ahi1* knockdown in both cell and animal models. Zebrafish embryos transiently express a ciliated structure called Kupffer's vesicle (KV) [30]. Cilia in KV generate a leftward fluid flow, which is fundamental for the development of left–right patterning and asymmetry during organogenesis [31]. Since the Ahi1 protein Jouberin localizes to the primary cilium/basal body complex [27], we were interested in evaluating the potential role of *ahi1* in KV formation and the subsequent development of left–right asymmetry [32]. *ahi1* knockdown in zebrafish led to a ciliopathy phenotype and multisystem disease, consistent with the human Joubert syndrome phenotype. Here we reveal the first evidence that *ahi1* knockdown in zebrafish embryos leads to loss of cilia from KV and subsequently altered cardiac left–right asymmetry. *ahi1* morphants also develop pronephric duct dilatation and cloacal abnormalities, in association with loss of cilia.

To extend these studies, we used a murine epithelial cell model to evaluate the function of Ahi1. Knockdown of *Ahi1* in murine renal epithelial cells prevented development of primary cilia from basal bodies and reduced the ability of cells to form adherens junctions with neighboring cells, leading to a disordered epithelium.

Together, this novel data emphasizes the important and extensive role of *AHI1* in development, from essential cellular signaling organelles, such as the primary cilium, to complex organ systems including the brain and the kidneys.

Methods

Sequence analysis

Putative Ahi1 orthologues were identified using a combination of reciprocal best BLASTP and iterative BLASTP as well as simple BLAST searches [33]. This initial search generated a very large number of false positives, which were only similar in terms of WD40 repeats. To overcome this problem, we performed further searches using human or *Naegleria gruberi* Ahi1 amino acids 1–540. These protein sequences were used to query the non-redundant predicted proteomes of 44 organisms (33 flagellate, 11 non-flagellate, Supplementary Table 1) chosen to represent a wide evolutionary spread of eukaryotes. Searches were carried out at NCBI (http://www.ncbi.nlm.nih.gov/) or JGI (http://www.jgi.doe.gov/) depending on the organism. An alignment was generated using MAFFT (Multiple Alignment using Fast Fourier Transform), trimmed to exclude the WD40 repeats and the low complexity N-terminal region, and displayed using GeneDoc (http://www.nrbsc.org/gfx/genedoc/) with "similarity group" shading in Conservation Mode. Pattern and profile searches were carried out used SMART, [34, 35] and Coils2 [36].

Zebrafish husbandry and genetic manipulation

Wild-type AB or *golden* zebrafish (ZF) were maintained and raised using standard animal husbandry. For zebrafish studies, all procedures were performed under Home Office UK license regulations. Embryos were kept at 28.5°C and 0.003% PTU (1-phenyl-2-thiourea; Sigma) was used to suppress pigmentation when necessary. Embryos were staged according to somite number for studying KV or hours post-fertilization (hpf) for later time points [37]. The *cldnb*:Lyn-GFP transgenic line (expressing Lyn-GFP driven by the *claudin-b* promoter) was a gift from Dr S. Burtey. *cldnb*:Lyn-GFP embryos express GFP at epithelial cell tight junctions with strong expression within the telencephalon, otic placode and pronephros (data not shown). To visualize cardiomyocytes and phenotype for cardiac looping abnormalities, we used transgenic zebrafish expressing GFP under control of the *cmlc2* (*myl7*) promoter (*cmlc2*:GFP) [38]. Splice (5′-CCACACTCTGAAAGGGAAAAACATT-3′) and translation (5′-GAGTCATTAGCAGCTTTGTTTTTCC-3′) blocking antisense morpholino oligonucleotides (MOs) were designed (Gene Tools, Philomath, Oregon, USA) to target zebrafish *ahi1* (NM_001077561). *Golden* and *cldnb*:Lyn-GFP transgenic zebrafish embryos (1–4 cell stage) were microinjected with between 0.5 and 6 ng MO diluted in Danieau solution and 0.5% phenol red. Mismatched control (5′-CCTCTTACCTCAGTTACAATTTATA-3′) and p53 (5′-GCGCCATTGCTTTGCAAGAATTG-3′) MOs were used in control experiments. Phenotypic rescue was performed by co-injecting 100 pg of in vitro transcribed mouse *Ahi1* mRNA (NM_026203) (mMessage Machine, Ambion) with *ahi1* splice or translation blocking MOs. Zebrafish were anesthetized with Tricaine solution and phenotyped at 56 hpf (to assess cardiac looping) and 72 hpf using morphology tables and severity scores. Images were captured using a fluorescent stereomicroscope (Leica MZ16F).

Zebrafish RNA isolation and RT-PCR

Total RNA was isolated from single ZF embryos from each experimental group at 24, 48, and 72 hpf. Embryos were anesthetized in Tricaine and washed in phosphate-buffered saline (PBS). A TissueRuptor (Qiagen) was used to homogenize tissue and a standard 1 ml Trizol (Invitrogen) protocol performed. Isolated RNA was resuspended in 10 µl RNAse-free water and quantified (Nanodrop ND-800 Spectrophotometer, Labtech). An equal concentration of RNA was used for each experimental group in reverse transcription (RT) reactions. Superscript VILO cDNA synthesis kit (Invitrogen) was used for RT. PCR using gene-specific primer pairs was performed: *ahi1* forward (5′-GAGGTCAGATGGGCTGTTTT-3′) and reverse (5′- AGACCCAGGCATAACTTTCG-3′) using an annealing temperature of 55°C and 35 cycles. Following electrophoresis, equal volumes of PCR products were visualized on 1.5% agarose gels. Bands were excised, purified (Qiagen) and directly sequenced (MWG Eurofins).

Whole-mount immunohistochemistry

Uninjected and *ahi1* MO injected *cldnb*:Lyn-GFP and *golden* ZF embryos were fixed at either 8–10 somite stage (in order to study KV) or 72 hpf, using 4% paraformaldehyde in PBS at 4°C overnight. To permeabilize embryos they were washed in ddH20 then pre-chilled acetone (−20°C) for 7 min. Embryos were washed in ddH2O and blocked in 5% bovine serum albumin, with 1% DMSO (Sigma) and 0.1% Tween. For cilial staining, embryos were incubated in primary antibody (mouse anti-acetylated tubulin antibody, 1:500, Sigma T6793) overnight at 4°C and detected using a donkey anti-mouse AlexaFluor594 conjugated secondary antibody (1:200, Invitrogen). For identification of KV epithelium, antibodies directed towards aPKC [39] were used (rabbit anti-aPKC (1:500, Santa Cruz) detected with goat anti-rabbit Alexa Fluor 488 conjugated secondary antibody (1:200, Invitrogen). Embryos were washed into PBS, mounted and imaged using confocal microscopy (LSM 510Meta, Zeiss and A1R Confocal, Nikon).

In situ hybridization and histology in zebrafish embryos

Whole-mount in situ hybridization was performed according to standard procedures [40] using *golden* ZF embryos. PCR primers used for generating zebrafish-specific *ahi1* in situ hybridization probes were: forward (5′-TCATTCGTGTACTGTGCCAAG-3′) and reverse (5′-CAACCTGGTCACCTGTCTCA-3′) (yielding a 544 bp PCR fragment). PCR fragments were cloned into pGEM-T Easy vector (Promega). Two additional *ahi1* riboprobes were generated using PCR with T7 and SP6 labeled oligonucleotides. Primer pair sequences were (5′-CAAGAGGAAGCTCCCACAAC-3′) and (5′-GGCTTTCTTTCGTGTCGATT-3′); (5′-AGGATGATGTAGAGGATTCAAGG-3′) (5′-CTCATAGAAGGATGAAACATGACG-3′), respectively.

Antisense and sense control probes were transcribed with SP6 or T7 RNA polymerase, respectively, and labeled using the DIG RNA labeling kit (Roche Diagnostics). The hybridization temperature was 65°C for all probes. A *charon* in situ hybridization probe (kind gift from Dr. Hibi) was used to localize KV epithelium [41]. Sonic hedgehog (*shh*) [42] and cardiac myosin light chain 2 (*cmlc2*) probes [43] were used as positive controls for zebrafish in situ hybridization experiments. For negative controls, a sense *ahi1* probe, a sense *charon* probe and no probe were used. Embryos were imaged using an Axioplan microscope (Axiocam HRC, Zeiss). For pronephric duct identification, following in situ hybridization protocols, ZF embryos were embedded in resin and sectioned at 5–8-µm intervals as described below. Sections were mounted before imaging using an axioplan microscope (Axiocam HRC, Zeiss).

For histological examination, ZF embryos were fixed at 72 hpf in 4% PFA in PBS at 4°C overnight. They were washed in DEPC-PBS at RT. Embryos were dehydrated by washing in ethanol series with DEPC-PBS (30, 50, 70, 90%) up to 100% ethanol. A standard resin embedding (Technovit, Heraeus Kulzer GmbH) protocol was performed and embryos were positioned in plastic moulds and allowed to set at 4°C for 48 h prior to sectioning at 5 µm using a microtome. The sections were mounted onto slides and stained using a standard methylene blue and fuchsin protocol [44]. Images were obtained using an axioplan microscope (Axiocam HRC, Zeiss).

Cell culture and siRNA using IMCD3 cells

Mouse inner medullary collecting duct (IMCD3) cells were cultured in DMEM/Ham's F12 supplemented with 10% fetal calf serum (Sigma-Aldrich, UK). For functional analyses, passage 13–20 IMCD3 cells were cultured on Transwell permeable supports (# 3431, Corning). For SEM studies, passage 13–20 cells were cultured on 13-mm glass cover slips.

Cells were transfected with a pool containing 100 pmol of each of four siRNA duplexes (OnTargetPlus SMART-pool, Dharmacon) against mouse *Ahi1* at 60–70% confluency using Lipofectamine 2000 according to the manufacturer's instructions. The medium GC non-targeting control (Invitrogen) was used as a negative control. siRNAs were as follows: oligonucleotide 1, 5′-GGUCAA AAGACGAUCGCUA-3′; oligonucleotide 2, 5′-UGAAGU UAGCCGCCGUGUAA-3′; oligonucleotide 3, 5′-GCUAA AUGUCGUCGAGGUU-3′; oligonucleotide 4, 5′-GUGAA ACACUGUAUCGAGA-3′. As a further control, siRNA studies were repeated with two individual siRNA oligonucleotides (numbers 2 and 3, above). All assays were carried out 96 h after transfection.

The following primary antibodies were used: anti-acetylated alpha tubulin clone C3B9 [45], rabbit anti-gamma tubulin (Sigma-Aldrich), rat anti-ZO-1 (MAB1520, Chemicon) and mouse anti-E-cadherin clone 36 (BD Transduction Laboratories). Secondary antibodies were: goat anti-mouse AlexaFluor488, goat anti-rabbit AlexaFluor594 (Molecular Probes) and goat anti-rat FITC (Jackson Immunoresearch). Western blotting was performed on whole-cell extracts to confirm siRNA efficiency as previously described [46].

We used mouse anti-AHI1 antibody at 1 in 500 dilution (ab93386, Abcam) together with rabbit anti-histone H3 (1:200) as a loading control. HRP-conjugated secondary antibodies (Dako) were used at 1:20,000. Blots were developed using Western Lightening enhanced chemiluminescence (Pierce) and scanned using Multi Gauge V2.2 software (Fujifilm) to determine relative band intensities.

Statistical analysis

Means and standard errors of means (SEM) were calculated using GraphPad Prism software. Results are presented as means $\pm$ SEM. For comparisons of phenotypes, contingency tables were generated. Fisher's exact test was used to compare two groups and Chi-squared test was used to compare more than two groups, with a level of significance at $p < 0.0001$.

Results

AHI1 encodes a ciliary/basal body protein which is highly conserved throughout evolution

The human *AHI1* gene encodes an 1,196 amino acid protein AHI1 (alias Jouberin), which is expressed in primary cilia and centrosomes of renal epithelial cells [27]. SMART domain analysis [34, 35] predicts several known protein domains including an N-terminal coiled-coil domain, six WD40 domains and a Src homology domain (SH3) (Fig. 1 and Supplementary Figure 1), which has recently been characterized using crystallography [47]. There is significant conservation of amino acid structure between human, mouse and zebrafish Ahi1 [48], with the exception of the absence of a predicted N-terminal coiled-coil domain [29] and an additional predicted WD40 domain in the murine isoform (Supplementary Figure 1).

Given the strong conservation of Ahi1 among vertebrates (Supplementary Figure 1) and its localization and likely role in primary cilia and basal bodies, we sought to identify additional homologues. We found that the nucleotide and protein sequences of Ahi1 are highly conserved throughout evolution (Fig. 1 and Supplementary Table 1). We searched the predicted proteomes of 44 eukaryotic organisms chosen to represent a wide evolutionary spread of organisms, including those that build a cilium or flagellum (33 organisms) and those that lack these structures (11 organisms). Despite having only been described in multi-cellular organisms to date, we report that Ahi1 evolved prior to the evolution of multicellularity and is conserved between ciliated protozoa and man.

We found a clear correlation between the presence of a predicted Ahi1 protein in genomes of organisms that build cilia or flagella, and absence in the genomes of organisms that do not build cilia or flagella (Supplementary Table 1). Moreover, putative Ahi1 orthologues were present in the genomes of organisms that build only sensory cilia (*Daphnia*, *Tribolium*) as well as in the genomes of organisms that build either motile cilia/flagella only, or both motile and sensory cilia. Interestingly, Ahi1 homologues were only found in the genomes of organisms that build a canonical nine triplet centriole (9 + 0) and were invariably absent from the genomes of organisms that have a specialized singlet or doublet centriole architecture. This implies a possible role for Ahi1 in building or maintaining a cilium from a triplet centriole.

ahi1 expression patterns during early zebrafish development reveal prominent retinal and brain expression

We examined *ahi1* expression in developing zebrafish using in situ hybridization in whole mount embryos.

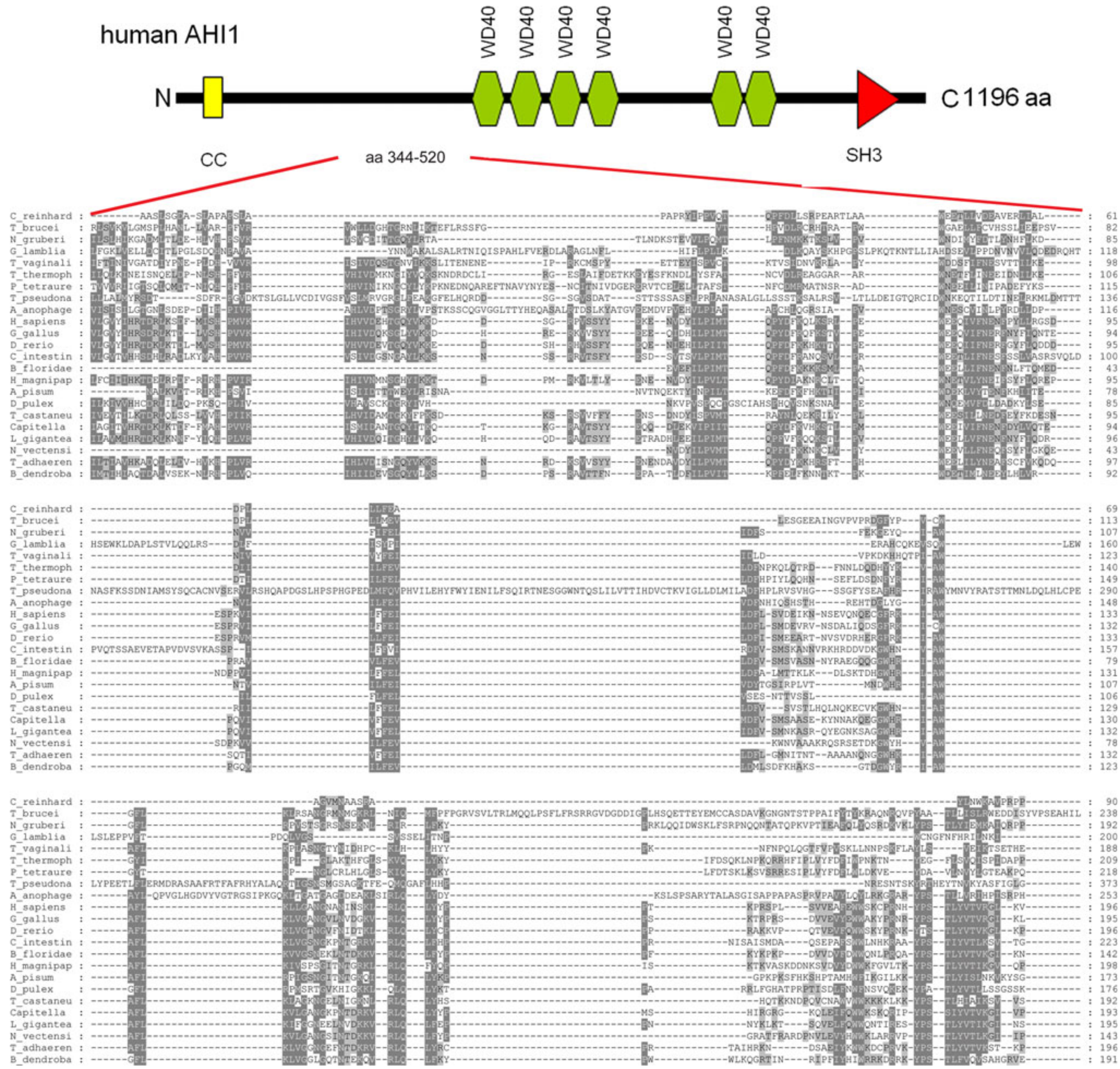

Fig. 1 Partial protein sequence alignment of predicted Ahi1 homologues in eukaryotes. The human AHI1 protein is shown schematically with known protein domains indicated. The alignment was trimmed relative to the human sequence as shown to display only amino acids 344–520, which demonstrate the presence of clear homologues outside the WD40 repeat region. Homology was determined by examination of candidate sequences including reciprocal BLASTP. *Shading* indicates conservation of amino acids with similar R groups. *Dark grey* denotes conserved in 50% of organisms; *mid-grey* denotes conserved in 30% of organisms; *light grey* denotes conserved in 10% of organisms. For full organism common and Latin names, see Supplementary Table 1

Identical patterns of *ahi1* expression were seen with 2 additional *ahi1* gene-specific riboprobes (data not shown). Negative controls omitting antisense riboprobe or using ahi1 sense riboprobes revealed very low levels of background staining (Supplementary Figure 2).

At the 8–10 somite stage, *ahi1* expression was seen at KV (Fig. 2a, b). As a positive control for the localization of KV, we show expression of *charon* (Fig. 2c, d), a known marker of KV [41]. Patterns of expression within KV of *ahi1* and *charon* are comparable. At the 8–10 somite stage *ahi1* expression is also seen in the developing retina (Fig. 2e). There is no prominent notochord expression of *ahi1*, especially when compared to expression of *shh* (Supplementary Figure 2J). At 24 hpf, the forebrain (telecephalon, diencephalon), mesencephalon (tectum) and hindbrain (cerebellum) show *ahi1* expression

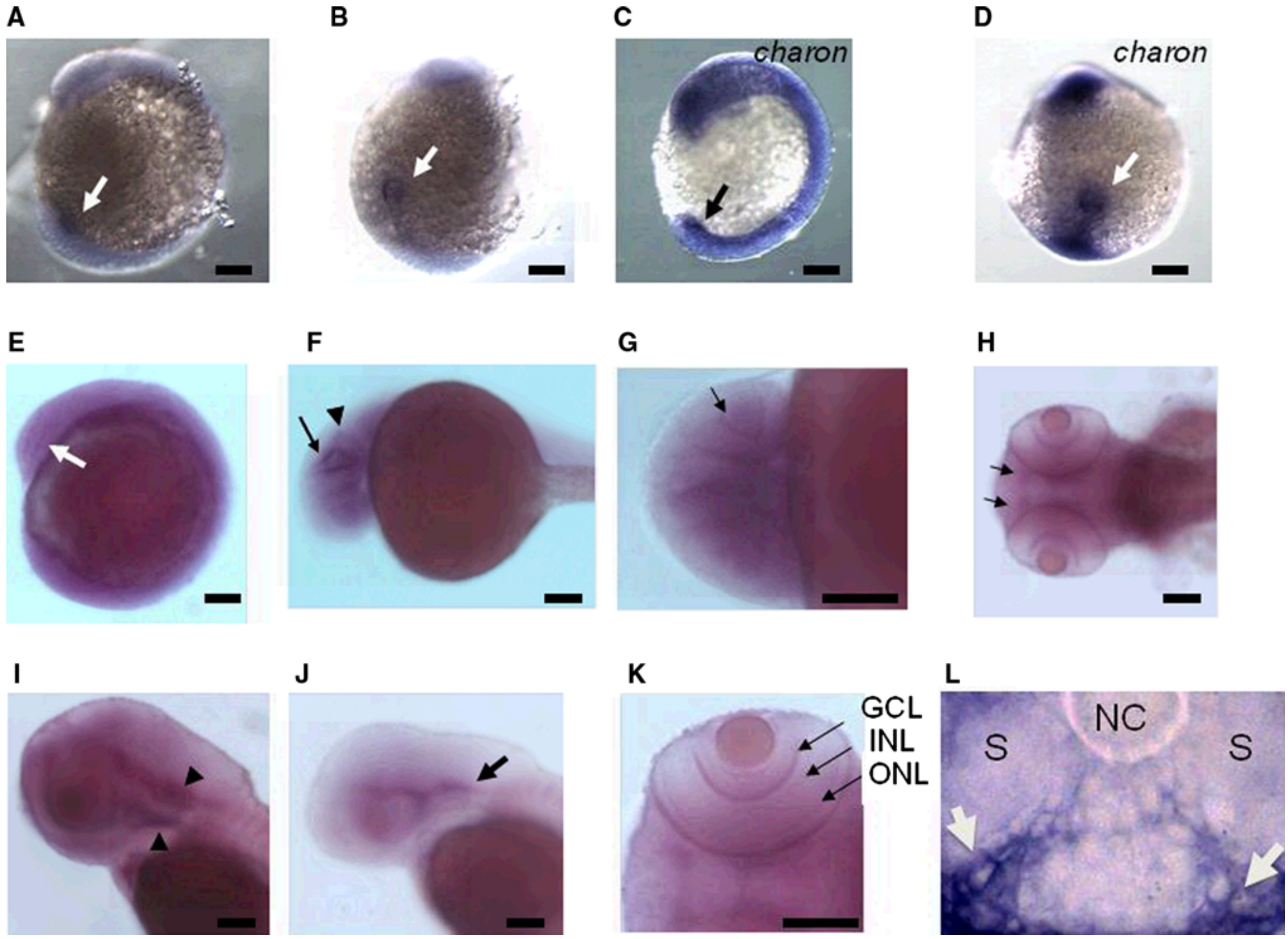

Fig. 2 *ahi1* expression during embryogenesis in zebrafish. *ahi1* expression studies in the developing zebrafish. Whole-mount in situ hybridization was performed using zebrafish embryos at **a**–**e** 12–14 hpf (8–10 somites), **f**, **g** 24 hpf, **h**, **i** 48 hpf and **j**, **k** 72 hpf. *Scale bar* 100 μm. Expression of *ahi1* is seen at KV, near the tailbud in lateral (**a**) and dorsal (**b**) views. Expression of *charon*, as a known marker of KV is shown for comparison (**c**, **d**). Retinal expression of *ahi1* is seen at 12 hpf (**e**, *white arrow*) while notochord expression is weak. At 24 hpf, the forebrain (telencephalon, diencephalon), mesencephalon (tectum, *arrow* in **f**) and hindbrain (cerebellum, *arrow head* in **f**) all show *ahi1* expression, together with retinal expression (*arrowed* in **g**). At 48 hpf *ahi1* is expressed in the hypothalamus and hindbrain (*arrows* in **h**) and inner ear (*arrowheads* in **i**). At 72 hpf *ahi1* expression continues to be seen in the inner ear (*arrowed* in **j**), olfactory bulbs and retina including the ganglion cell layer (GCL), inner nuclear layer (INL) and outer nuclear layer (ONL) (*arrowed* in **k**). **l** A transverse section of a 48 hpf embryo following in situ hybridization with *ahi1* probe, demonstrates expression of *ahi1* in the distal pronephros (*white arrows*). *NC* notochord; *S* somites

(Fig. 2f) in addition to strong retinal expression of *ahi1* (Fig. 2h). At 48 hpf, *ahi1* was expressed in the olfactory bulbs, retinal layers and inner ear (Fig. 2h, i). At 72 hpf, *ahi1* expression continues to be prominent in the inner ear (Fig. 2j), functional retina (ganglion cell layer, inner nuclear layer and outer nuclear layer) and olfactory bulbs (Fig. 2j, k). In order to establish whether *ahi1* was expressed in the developing pronephros, we used *ahi1* in situ hybridization in whole mount 48 hpf embryos followed by resin embedding and tissue sectioning. We demonstrate *ahi1* expression within the pronephric ducts (Fig. 2l), with prominent expression seen at the apical (luminal) surface.

Knockdown of *ahi1* in zebrafish reveals phenotypes typical of a ciliopathy

Antisense morpholino oligonucleotide injections targeting the *ahi1* ATG initiation codon (ATG MO) and an internal splice donor sequence of exon 8 (SPL8 MO) both caused defects in convergent extension, eye, hindbrain and ear development (Fig. 3e–o), as well as cyst formation in the pronephric kidney tubules (Fig. 3g, h, i, r). A variety of otic vesicle abnormalities were observed, with either absent, single or triple otoliths (Fig. 3j–o). These abnormal developmental phenotypes are comparable to the clinical features seen in humans with JSRD caused by *AHI1*

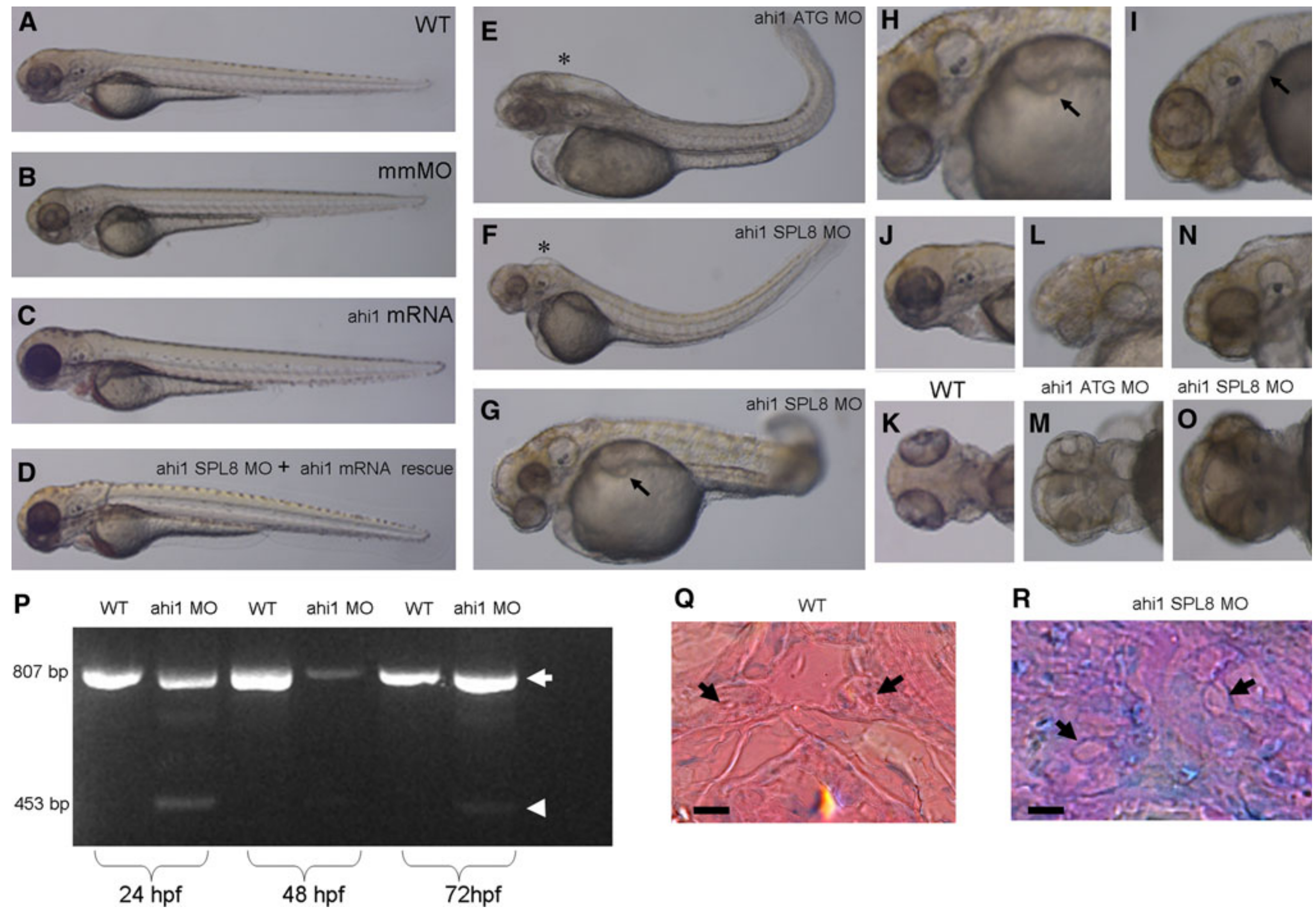

Fig. 3 *ahi1* knockdown in zebrafish recapitulates a ciliopathy phenotype. *ahi1* MO-injected embryos show a range of dysmorphology. Lateral views of 72 hpf embryos including **a** wild-type (WT) uninjected, **b** mismatched MO injected, **c** murine *Ahi1* mRNA injected and **d** rescue of *ahi1* MO-injected embryo with murine *Ahi1* mRNA were phenotypically normal. **e** 4 ng of *ahi1* translation blocking MO-injected embryo (*ahi1* ATG MO) and **f**, **g** 1 ng *ahi1* SPL8 MO-injected embryos demonstrate curved body axis, hydrocephalus (*asterisk*), **h** coloboma with abnormal eye development, pericardial edema and pronephric cysts (indicated by *arrow*, **g**–**i**). **h**, **i** Zoomed views of *ahi1* SPL8 MO-injected embryos demonstrating pronephric cysts (indicated by *arrow*). Lateral (**j**, **l**, **m**) and dorsal (**k**, **m**, **o**) views of otic placode. **j**, **k** Wild-type otic placode containing two otoliths, **l**, **m** empty otic placode in *ahi1* ATG MO-injected embryo, **n**, **o** single otolith in *ahi1* SPL8 MO-injected embryo. **p** RT-PCR of mRNA from single WT (expected size 807 bp, arrowed) and *ahi1* SPL8 MO-injected embryos at 24–72 hpf revealing abnormal splicing of mRNA (band seen at 453 bp, arrow head) with an in-frame deletion of exon 8 (354 bp). A maximal knockdown of ahi1 is seen at 48 hpf, with some recovery of wild-type RT-PCR product at 72 hpf. **q**, **r** Resin sections of WT, and *ahi1* SPL8 MO-injected embryos at 72 hpf (*black arrows*, pronephros). **q** WT undilated pronephros. **r** Mildly dilated pronephros (*black arrows*) induced by *ahi1* SPL8 MO. *Scale bar* 10 µm

mutations, with a preponderance towards central nervous system defects, and milder renal phenotypes [4, 9, 23–26]. A mismatch control morpholino (mmMO) had no effect on nervous system development or renal cyst formation (Fig. 3b). Co-injection of murine *Ahi1* mRNA with the *ahi1* SPL8 MO completely rescued the morphant phenotype (Fig. 3d), suggesting specificity of the *ahi1* knockdown. RT-PCR of 24–72 hpf embryos following *ahi1* SPL8 MO injection demonstrated a splicing defect (Fig. 3p) with a PCR product of 453 bp reduced from 807 bp, with maximal knockdown occurring after 48 hpf. Direct sequencing confirmed skipping of exon 8 and introduction of a premature stop codon (data not shown). A modest dilatation of the proximal pronephros was seen in *ahi1* SPL8 MO-injected embryos, with lumen diameter 5–10 µm, when compared to WT proximal pronephros diameter of 3–5 µm (Fig. 3q, r).

Given the strong retinal expression seen with *ahi1* in situ hybridization (Fig. 2) and the presence of abnormal eye shapes in *ahi1* morphants (Fig. 3), we carried out histological analysis of the retina using control and *ahi1* morphants at 72–120 hpf. We observed a defect in lamination of the cell layers of the retina including the ganglion cell layers and the inner and outer nuclear layers in *ahi1* morphants. This was in contrast to control embryos, where normal lamination was seen (Supplementary Figure 3). The development of the retinal pigment epithelium (RPE) however appeared normal in *ahi1* morphants.

To quantify the phenotypes of *ahi1* morphants, we examined developing embryos at 72 hpf. The most common phenotype observed following *ahi1* knockdown was body axis curvature ("curly tail"), occurring in a dose-dependent manner, in a mean of ~27% and ~12% of morphants injected with 6 and 3 ng of *ahi1* ATG MO, respectively (Supplementary Figure 4A). Similarly, a curly tail phenotype was seen in ~43 and ~39% of morphants injected with 2 and 1 ng *ahi1* SPL8 MO, respectively (Supplementary Figure 4B). We also observed dose related defects of the nervous system (hydrocephalus) in a mean of 12 and 3% of embryos with 6 and 3 ng *ahi1* ATG MO injection, respectively (Supplementary Figure 4A). Similarly, hydrocephalus was seen in a mean of 31 and 22% of embryos with 2 and 1 ng *ahi1* SPL8 MO injection, respectively (Supplementary Figure 4B). Generally, all the phenotypic anomalies were more prevalent with *ahi1* SPL8 MO rather then *ahi1* ATG MO injection, with a dose related response consistently evident (Supplementary Figure 4A,B). Higher doses of *ahi1* SPL8 MO (up to 6 ng) were attempted in order to induce an increased frequency of abnormal phenotypes, particularly of pronephric cysts. However, such doses led to an excess of mortality at 24 hpf (Supplementary Figure 4C).

Complete rescue of the morphant phenotype (indistinguishable from uninjected wild-type) occurred in 89% of embryos ($n = 62$) embryos following co-injection of *ahi1* MO with murine *Ahi1* mRNA compared to 21% ($n = 106$) of embryos with a wild-type phenotype following injection with *ahi1* MO (Supplementary Figure 4D, $p < 0.0001$, Fisher's exact test). For each phenotype, mRNA rescue of *ahi1* knockdown showed a significant reduction ($p < 0.0001$, Fisher's exact test) of numbers of embryos displaying the abnormal phenotype (Supplementary Figure 4E).

Knockdown of *ahi1* in zebrafish reveals a loss of cilia at Kupffer's vesicle and a reversal of cardiac looping

Developing zebrafish transiently express a ciliated structure called KV [30], which is the equivalent of the mouse embryonic node and important in establishing left–right patterning. We looked for abnormalities in cilia in KV following *ahi1* MO injection. Under light microscopy at the 8–10 somite stage, KV is visualized in uninjected control and *ahi1* morphant embryos, evident in both lateral and dorsal views (Supplementary Figure 5A,B,D,E). KV remains intact and morphologically preserved. Using an in situ hybridization probe directed towards *charon*, a KV-specific marker [41], we confirm that there is no change in the expression pattern within KV in *ahi1* morphants compared to control uninjected embryos (Supplementary Figure 5C,F).

Fig. 4 Loss of cilia at Kupffer's vesicle in *ahi1* morphant zebrafish ▶ embryos. **a–f** *cldnb*:Lyn-GFP transgenic zebrafish embryos were fixed at the 8–10 somite stage and labeled with anti-acetylated tubulin (*red*) for visualization of cilia at Kupffer's vesicle (KV). **a–c** Uninjected embryos show *cldnb*:Lyn-GFP expression (*green*) at cell–cell junctions of epithelial cells within KV, with a ciliated (*red*) apical surface. **d–f** *ahi1* SPL8 MO injected embryos demonstrate disorganized *cldnb*:Lyn-GFP expression at KV (*green*) and a loss of cilia. **g–l** Fluorescent immunostaining of *golden* zebrafish *ahi1* morphant embryos fixed at 8–10 somite stage and labeled with aPKC antibodies (*green*) to identify KV epithelium and anti-acetylated tubulin (*red*) for visualization of cilia. **g–i** An intact KV epithelium, with normal labeling of aPKC and preserved cilia expression. **j–l** A disrupted KV epithelium with diffuse aPKC signal and almost complete absence of cilia. *Scale bar* 20 μm

We next performed immunostaining using an acetylated tubulin antibody to study cilia, on control and *ahi1* morphants at the 8–10 somite stage. We demonstrated in *cldnb*:Lyn-GFP embryos, that KV is present and was ciliated in control embryos (Fig. 4a–c). However, in *ahi1* morphants, while KV was identified using *cldnb*:Lyn-GFP fluorescence (Fig. 4d) there was some disorganization of the usual expression pattern of *cldnb*:Lyn-GFP, together with loss of cilia from KV (Fig. 4d–f). In repeated experiments using embryos of 8–10 somites, cilia were absent from KV in 23 out of 25 (92%) *cldnb*:Lyn-GFP embryos following *ahi1* MO injection (Supplementary Figure 6A).

In order to further assess this apparent disruption to the development of KV in *ahi1* morphants, we injected *golden* embryos with *ahi1* MO and used primary antibodies directed towards aPKC, a marker of the apical membranes of KV cells [49], in combination with the ciliary marker, acetylated tubulin. In 8–10 somite embryos we were able to visualize KV, using aPKC staining (Fig. 4g–l). Some *ahi1* morphants had a preserved KV appearance with a normal aPKC staining pattern and preserved cilia (Fig. 4g–i). While in some other *ahi1* morphants, there was a less distinct pattern of aPKC staining, associated with almost complete absence of KV cilia (Fig. 4j–l).

Cilia within KV help to generate a leftward fluid flow, termed nodal flow [31]. This initiates a set of molecular signals which determines laterality. Since we have shown that cilia are absent within KV in *ahi1* morphants, we hypothesized that this would lead to a defect in organ laterality. We therefore examined developing embryos for abnormalities in cardiac asymmetry.

The normal zebrafish heart extends initially from the midline to the left side in approximately 97% of embryos, before looping places the ventricle closer to the midline and ultimately to the right of the atrium (D-loop) by approximately 48 hpf. Usually, in up to ~2% of embryos this is reversed (L-loop) and in 1% the heart remains in the midline (no loop) [50, 51]. Aberrations of left–right asymmetry are associated with an increased frequency of

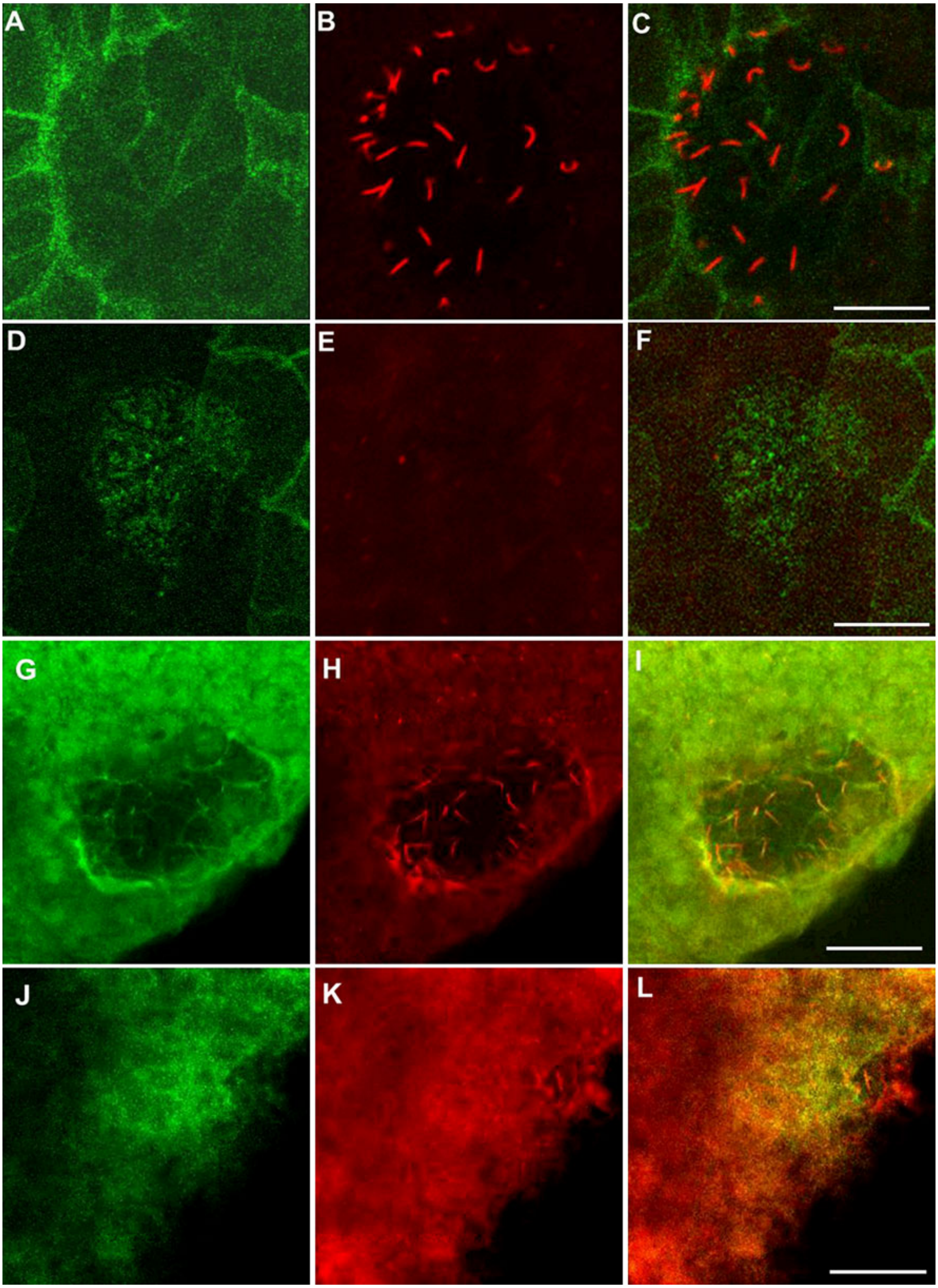

reversed loops (L-loop) or no loop (when the heart tube remains straight and often lies in the midline) [32].

In uninjected control zebrafish embryos examined at 56 hpf ($n = 145$), the heart was seen to loop towards the right in 100% of embryos (Fig. 5). Strikingly, in *ahi1* injected embryos ($n = 221$), 68% of embryos demonstrated reversed cardiac looping, with the heart in a L-loop pattern, 6% of embryos showed no looping, while 26% of

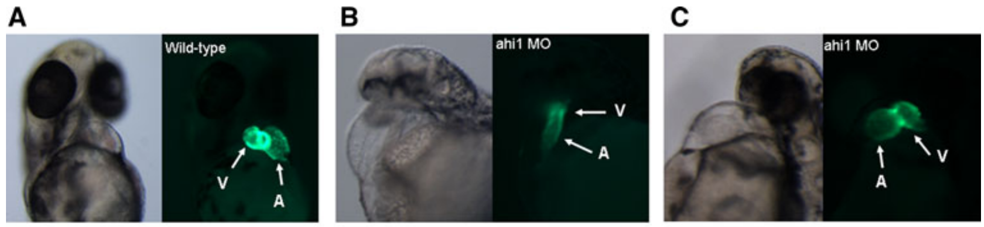

D

Cardiac looping (%)

Group	n	D-loop	No loop	L-loop
Wt	145	100	0	0
ahi1 MO	221	26	6	68
mm MO	39	97	0	3

Fig. 5 Heart laterality defects after *ahi1* knockdown. Paired brightfield and GFP fluorescence images are shown of *cmlc*2-GFP zebrafish embryos at 56 hfp. Examples of **a** normal D-looping of heart in uninjected embryos, **b** no loop, and **c** L-looping in *ahi1* SPL8 MO injected embryos are shown. Ventricle, *V* and atrium, *A* are *arrowed*. **d** Summary table of cardiac looping defects

ahi1 morphants showed the normal phenotype of D-looping (Fig. 5 and Supplementary Figure 6B). Mismatch morpholino (mmMO) injection produced a normal pattern of heart looping (Fig. 5d).

Knockdown of *ahi1* in zebrafish is associated with pronephric duct and cloacal dilatation and loss of pronephric cilia

Using *cldnb*:Lyn-GFP transgenic zebrafish, using fluorescent microscopy, we visualized the epithelium of the pronephric ducts. In uninjected control embryos, ciliated pronephric ducts, with a non- dilated lumen and a uniform columnar epithelium were observed (Fig. 6a–c). In mismatched MO injected fish no cystic dilatations were observed (data not shown). However, *ahi1* morphants displayed a range of phenotypes. Figure 6d–f demonstrate cloacal dilatation (Fig. 6e, asterisk) where the expression pattern of *cldnb*:Lyn-GFP in the pronephric ducts was preserved, together with preserved cilia within the pronephros (Fig. 6d, arrowed). In *ahi1* morphant embryos with more severe phenotypes, *cldnb*:Lyn-GFP expression in the pronephros appeared disorganized, with dilatation of the pronephros and an absence of cilia within the pronephric duct (Fig. 6g–i).

Knock down of *Ahi1* in IMCD3 cells leads to a reduction in primary cilia and cell polarity defects

Given our data showing the requirement of *ahi1* for ciliogenesis in KV and the pronephros of the zebrafish, we tested the effect of gene silencing of *Ahi1* on ciliogenesis in murine collecting duct cells. We used a pool of four siRNA duplexes targeted against *Ahi1*, as well as two individual duplexes. siRNA was transiently transfected into IMCD3 renal epithelial cells, and the presence of cilia assessed 96 h later using anti-acetylated α-tubulin antibody as a ciliary marker. We used Western blotting to determine that siRNA had been successful (Fig. 7d). In contrast to wild-type (data not shown) and negative control siRNA-transfected cells, ciliary formation was reduced in *Ahi1*-silenced cells (Fig. 7a–c), although centrioles/basal bodies could still be observed with anti-γ-tubulin antibody (Fig. 7a). Ciliary formation was significantly reduced ($p < 0.0001$, Chi-square test) on silencing of *Ahi1*: 74% of negative control-transfected cells showed ciliary staining, while *Ahi1*-silenced cells using a pooled Ahi1 siRNA displayed cilia in only 24% (Fig. 7b). In addition to an absence of primary cilia, scanning electron microscopy revealed an indistinct pattern of cell–cell boundaries in *Ahi1* siRNA-treated cells (Fig. 7c), suggesting a problem with formation of a polarized epithelium. The establishment of cell–cell contacts is essential for epithelial polarity and tissue morphogenesis [52, 53]. We therefore tested the effect of *Ahi1*-silencing on the distribution of the tight-junction marker ZO-1 and the adherens junction marker E-cadherin and found an abnormal appearance of E-cadherin in *Ahi1* siRNA-treated cells compared to control cells (Fig. 7e). In contrast, there was no apparent difference in tight junction appearance (Fig. 7f). Only one nucleus was generally visible per ring of tight junctions (Fig. 7f), indicating that the lack of cell boundaries at the apical surface is not due to multinucleated cells, and suggesting that cytokinesis failure and cell fusion are not features of the phenotype.

Discussion

WD40 repeats are enriched in ciliary and basal body proteins [54] and although Ahi1/Jouberin was not identified as part of this predicted flagellar and basal body proteome [54], it has subsequently been identified as a member of the ciliary proteome [55], and a member of the photoreceptor sensory cilium complex [56].

Additional evidence for a ciliary role for Ahi1 was provided by the localization of Ahi1 to the mother centriole and

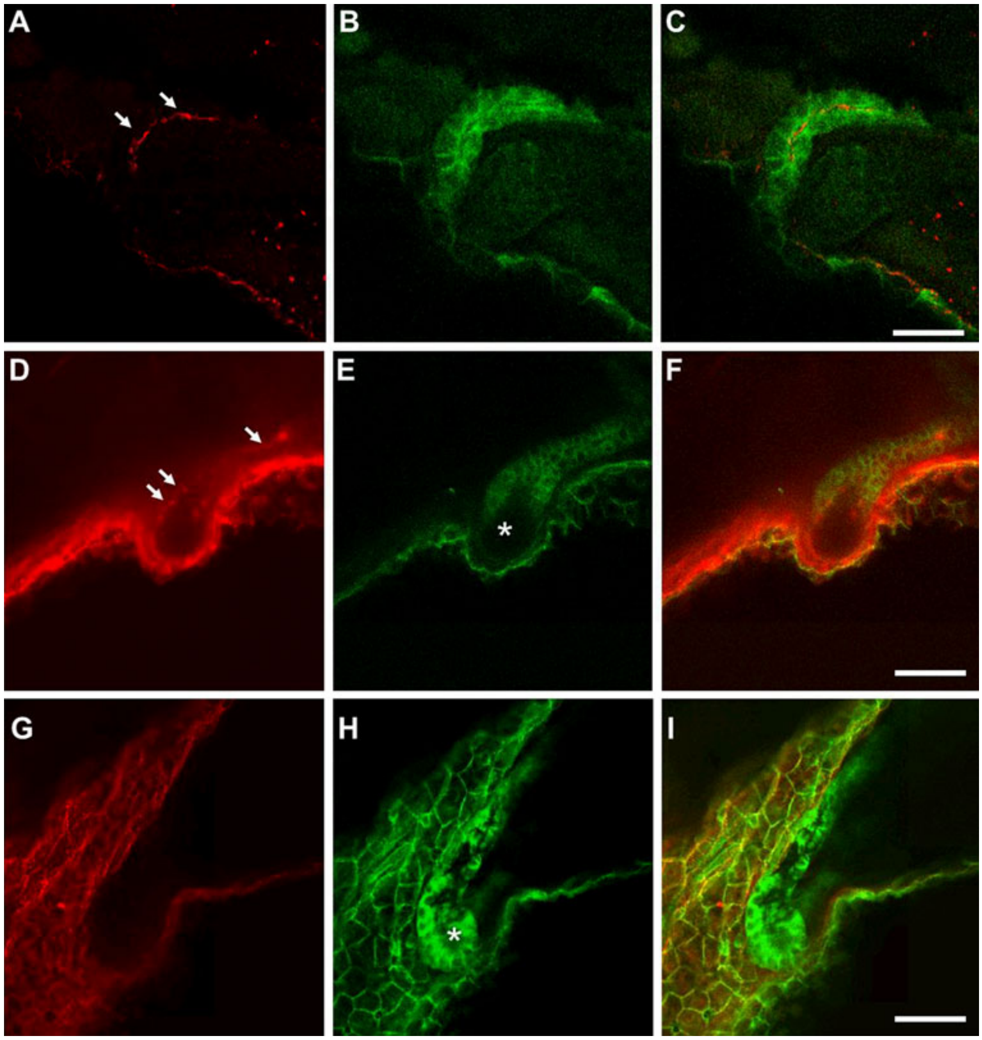

Fig. 6 Pronephric duct dilatation and absent cilia in *ahi1* morphant zebrafish embryos. Fluorescent immunostaining of *cldnb*:Lyn-GFP transgenic zebrafish embryos at 72 hpf using anti-acetylated tubulin antibody (*red*), as a cilial marker. **a–c** Uninjected control zebrafish embryos demonstrate a ciliated pronephros (**a**, *arrowed*) with *cldnb*:Lyn-GFP expression seen in a columnar epithelium (**b** and overlay **c**). **d–i** *ahi1* SPL8 MO-injected embryos demonstrate a spectrum of severity with dilatation of the pronephric ducts (**e** and **h**, *asterisk*), with disordered *cldnb*:Lyn-GFP expression and either a preservation of cilia (**d** and overlay **f**) or an absence of cilia (**g** and overlay **i**). *Scale bar* 50 μm

the basal body [57]. Using a bioinformatics approach, we have confirmed a pattern between Ahi1 expression and ciliated organisms (Supplementary Table 1). Similar profiles have previously been observed for flagellar proteins [54, 58, 59], suggesting that the localization of Ahi1 to the mother centriole and the basal body [57] is functionally significant. These in silico data indicate that Ahi1 is an ancient protein that appeared prior to the evolution of multicellularity suggesting that Ahi1 may play a role in forming both motile and sensory cilia. The presence of a predicted Ahi1 homologue in the *Aureococcus anophagefferens* genome is interesting, as this organism is not known to have a flagellate life-cycle stage [60, 61]. No centrioles have been observed in *Aureococcus* to date; however, the *A. anophagefferens* genome does have components of the core centriole [62] and it has been proposed to have a flagellate stage in its life-cycle based on the presence of flagellar components in its genome [61, 63, 64]. Our genomic analysis showing the presence of an Ahi1 homolog in *A. anophagefferens* is entirely consistent with this idea. We also found a markedly divergent Ahi1-like sequence in *Thalassiosira pseudonana*. The centriole architecture for this organism is unknown; however other centric diatoms build a doublet centriole [65]. This might indicate that *Thalassiosira* is an exception to the restriction of Ahi1 to the genomes of organisms that build a triplet centriole. Ultrastructural analysis of centriole architecture in this organism will be needed to see if this is indeed the case.

Consistent with previous studies [57], we did not observe a complete abolition of ciliogenesis in siRNA-treated IMCD3 cells, but rather a significant reduction in the number of primary cilia observed. Similar experiments using siRNA knockdown of ciliopathy genes in IMCD3

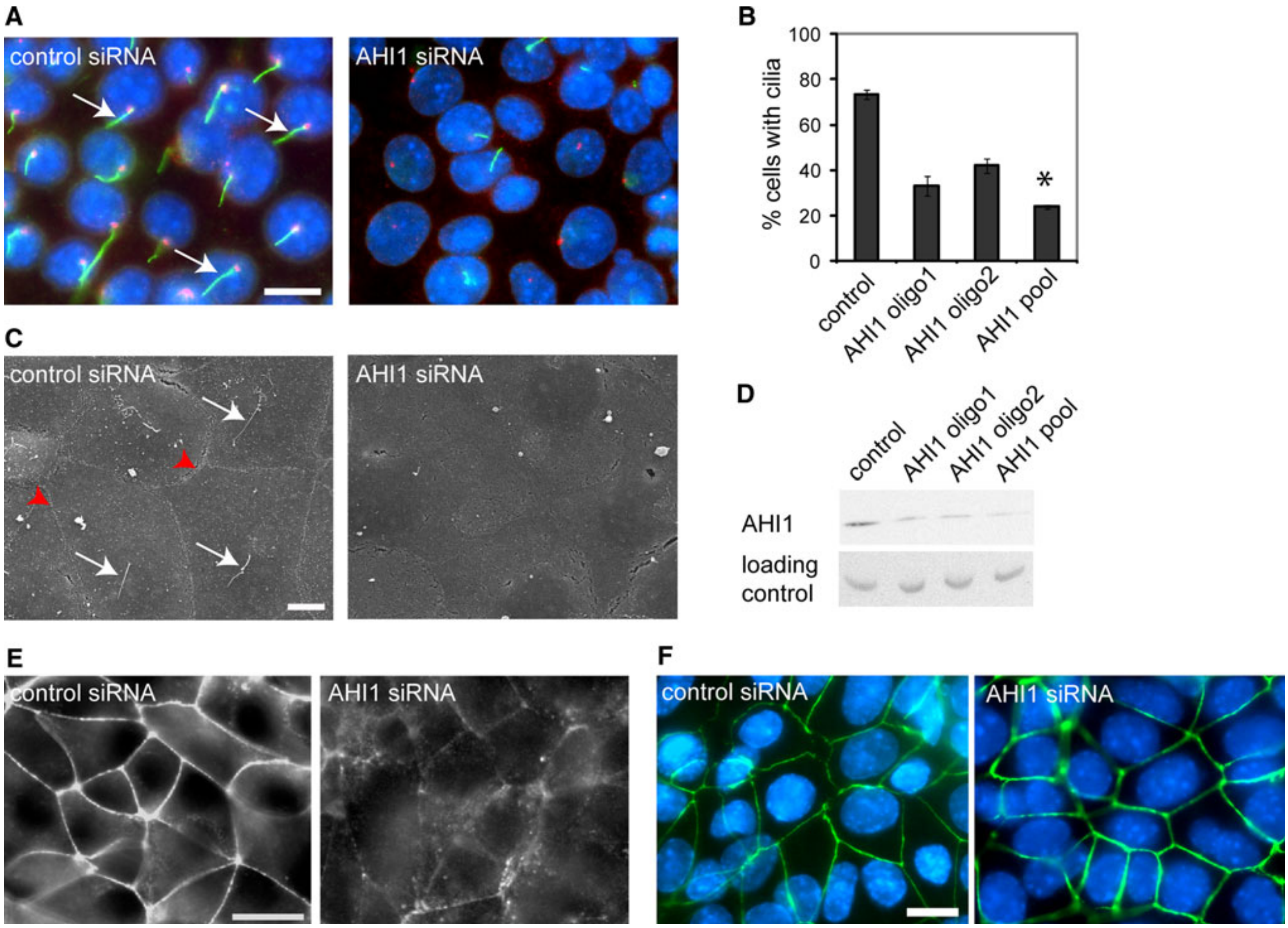

Fig. 7 siRNA-mediated knockdown of *Ahi1* causes loss of cilia and cell polarity defects. Immunofluorescence (**a**, **e**, **f**), scanning electron microscopy (**c**) and Western blot (**d**) of IMCD3 monolayers transfected with negative control siRNA or siRNA against *Ahi1*. **a**, **b** Loss of primary cilia (acetylated alpha-tubulin staining, *green*) in *Ahi1*-silenced cells (*right panels*) compared to the cilia seen in control-transfected cells (*left panel*, *white arrows*). DNA is labeled with DAPI (*blue*) while the centrosome (gamma-tubulin staining) is shown in *red*. **b** Quantification of primary cilia in transfected cells. At least 1,500 cells were counted for each condition; $n = 5$ experiments. In control-treated cells, 74% were ciliated, while 24% of cells were ciliated following treatment with pooled AHI1 siRNA (*, $p < 0.0001$, Chi-square test). **c** As well as the loss of primary cilia seen in control cells (**c**, *left panel, white arrows*), *Ahi1*-silenced cells failed to properly differentiate the apical cell surface. Very few microvilli were present and cell–cell boundaries were indistinct compared to those in control cells (*left panel, red arrowheads*). **d** Western blot showing success of siRNA. The pooled siRNA sample showed an 87% reduction in band intensity relative to the control, while the individual siRNAs gave a reduction of 72 and 69% for AHI1 oligo 1 and AHI1 oligo 2, respectively. **e**, **f** Aberrant appearance of adherens junctions (**e**, E-cadherin staining) in *Ahi1*-silenced cells compared to the control; in contrast tight junctions (**f**, ZO-1 staining in *green*, DAPI in *blue*) appear normal. NB: all *Ahi1* siRNA images show cells transfected with a pool of siRNAs. *Scale bars* 5 µm

were recently reported [22]. Here, siRNA targeting Ahi1 did not lead to a significant change in ciliogenesis, rather a modest defect in spheroid growth in 3D culture was observed, suggesting a role for Ahi1 in tissue apical organization as well as other yet to be defined roles [22]. The restriction of Ahi1 to the genomes of organisms that build a canonical nine triplet microtubule centriole might be indicative of a role for Ahi1 in building or maintaining a cilium from a triplet centriole and signaling pathways specific to this structure. Given the cilium phenotype described here and previously [57], it will be interesting to examine the ultrastructural appearance of centrioles in *Ahi1*-mutant cells to see if centriole maturation or acquisition of the accessory structures that characterize a mature basal body are compromised. Alternatively, there could be a problem with formation of the ciliary vesicle in *Ahi1*-mutant cells or Ahi1 could play a role in the construction of the axoneme itself.

In work dating back nearly 60 years, Sorokin described the formation of cilia, which required three stages [66]. This included an initial phase where a “primary vesicle” appears at the end of a centriole. Following attachment of this vesicle, a “ciliary bud” is formed. Secondly, the ciliary shaft develops and elongates; a postulated requirement for this is the addition of ciliary vesicles which fuse to the primary vesicle. Finally, there is "emergence" of the cilium to the cell surface and its protrusion out of the cell [66]. More recently, the depression in the plasma membrane in which the cilium sits, known as the ciliary pocket, has been elegantly described [67] in both renal and retinal epithelial cells. This structure may be important in regulating vesicular traffic and is intimately related to the actin cytoskeleton. Given that Ahi1 interacts with Rab8a, a small GTPase, and this interaction is required for ciliogenesis and vesicular trafficking [57], it seems that Ahi1 function might be critical to the ciliary pocket and the conserved protein domain structure of Ahi1 is consistent with a role as a scaffolding protein [9] at this location.

However, it is possible that Ahi1 might have multiple roles in cells. Our data in IMCD3 cells suggest that Ahi1 is required for formation of adherens junctions and subsequent apical–basal polarity. In IMCD3 cells, the Ahi1 siRNA treatment dramatically decreased the staining of the cell–cell contact areas as demonstrated by anti-E-cadherin staining. In contrast, the tight junctions, by anti-ZO-1 staining showed no abnormality. Formation of apical–basal polarity and cell–cell junctions are both dependent on an intact actin cytoskeleton, and the disruption of adherens junctions is consistent with the idea that Ahi1 also plays a role in establishing or responding to cell polarity via the formation and organization of cytoskeletal networks [57]. Recent data suggests that Ahi1 may act as a potential bridging molecule between other nephrocystin proteins, given AHI1 interacts with NPHP2, MKS1, MKS6, and Tectonic-1 [22]. There is also increasing evidence for non-ciliary roles for proteins previously thought of as having a purely ciliary function [68]. Examination of the publicly available EST databases suggests expression of a number of different Ahi1 isoforms and it is possible that different isoforms fulfill different cellular roles. Alternatively, Ahi1 might play different roles in different cellular locations, as has been demonstrated for the "ciliary" cation channel polycystin-2 [69]. While the localization described for Ahi1 is to the mature centriole [57], many proteins undergo highly dynamic changes in their localization that are not observed by immunofluorescence. Live-cell imaging of tagged Ahi1 will be required to test if this is the case.

We have demonstrated prominent early embryonic expression of *ahi1* in zebrafish where *ahi1* is expressed in KV, a ciliated organizing structure, as well as in multiple tissues, including the developing brain and eye. We have also established that *ahi1* is present in the developing pronephros. Previous expression studies in murine tissues showed *Ahi1* expression in neurons of the developing hindbrain, midbrain and forebrain, pituitary, testis, and kidney [29]. *Ahi1* expression in murine brain has been reported during early embryonic life (day 10.5) and persisted into adult life. A role for Ahi1 in neurons and neuronal function is implicated given the fact that all the major anatomical defects in JBTS involve brain structures [6, 9, 23, 29, 70, 71]. In contrast, in a recently described murine model ($Ahi1^{-/-}$), the brain morphology was grossly preserved [26] and neuronal-specific Nestin-Cre conditional *Ahi1* knockout mice survived to weaning, suggesting a role for Ahi1 outside of the CNS, which affects survival [26]. Murine Ahi1 interacts with Huntingtin-associated protein 1 (Hap1) and consistent with a role for Ahi1 in cerebellar development, Hap1-knockout mice showed reduced Ahi1 levels, abnormal cerebellar development and abnormal axonal decussation [72]. There is evidence that *AHI1* mutations and polymorphisms may modify the brain phenotype of JBTS patients [28].

Consistent with a role of *ahi1* in the epithelium of the pronephric ducts, we have shown that using zebrafish to model JSRD, *ahi1* morphants may develop renal cystic disease, pronephros dilatation and cloacal abnormalities. We have previously noted this pattern of cloacal disruption in *nphp6* (alias *cep290*) morphants [12]. Given the zebrafish pronephros is segmented in a similar manner to the human nephron [73], a dilatation of the most distal pronephric segments is consistent with cortico-medullary cyst formation as seen in patients with nephronophthisis [74]. The absence of cilia within the pronephros of some *ahi1* morphants is in keeping with the complete loss of cilia within KV of *ahi1* morphants and the significant reduction of cilia in siRNA-treated IMCD3 cells. In addition, the irregular expression pattern of *cldnb*, suggests a disruption of the distal pronephros epithelium in *ahi1* morphants. This, together with aberrant appearance of adherens junctions in siRNA-treated IMCD3 point towards *Ahi1* mediating alterations in epithelial morphogenesis, cell adhesion and polarity.

The most common phenotype we observed in *ahi1* morphants was a defect in body axis leading to curvature ("curly tail"), in association with defects of left–right asymmetry, edema and pronephric cysts. Typically, such phenotypes are seen in zebrafish with loss of intraflagellar transport proteins, which are required for cilia assembly [75]. Other models of ciliopathies in zebrafish also show "curly tails" alongside defects in cilia length or motility, left–right defects and pronephric cysts [76–79]. The *ahi1* morphant "ciliopathy" phenotype we describe is consistent with the demonstrated defect in cilia formation at KV and in the pronephros of *ahi1* morphants. Other similar zebrafish models of JBTS demonstrating combinations of hydrocephalus, body axis curvature and pronephric cysts have been reported including *nphp6* [12], *arl13b* [76], *cc2d2a* [18] and *cxorf5* [80].

We show that a likely consequence of the lack of cilia and abnormal KV in *ahi1* morphants is the dramatic change in cardiac looping, with a significant reversal of the normal D-looping pattern (Fig. 5). Situs inversus has been described in a small number of patients with mutations in ciliopathy genes, including *NPHP2* [81], *NPHP3* [82] and *NPHP6* [13]. Although we are not aware of patients with *AHI1* mutations and situs inversus, other cardiac defects are often noted, such as atrial septal defects [23].

Our data confirms *ahi1* expression during retinal development during zebrafish embryogenesis, with a disruption of *ahi1* in the zebrafish leading to loss of retinal lamination. Consistent with the severe retinal phenotype we describe in *ahi1* morphants, elegant studies in murine models have confirmed that *Ahi1* is a modifier of retinal phenotype [26]. The $Ahi1^{-/-}$ mice demonstrated a rapid loss of outer nuclear layers by 1 month of age. Electron microscopy revealed that photoreceptor ciliary axonemes were intact, with a preserved 9 + 0 microtubular doublet configuration [26]. This suggests that Ahi1 is not involved in the structural development of the photoreceptor axoneme, but rather may have functional consequences and affects the photoreceptor cell maintenance and survival.

In conclusion, we have demonstrated in early zebrafish development an expression pattern for *ahi1* which includes KV, neuronal and retinal structures, and the developing pronephric ducts. *ahi1* morphant zebrafish recapitulate the human JSRD phenotype with structural brain defects, retinal dystrophy and renal cysts. We provide novel evidence of disruption of the ciliated organizing center KV and consequently altered left–right patterning in ZF embryos. In both the zebrafish pronephros and renal epithelial cells we confirm a requirement for Ahi1 in ciliogenesis and cell–cell junction morphology suggesting roles for Ahi1 in the development and maintenance of these structures.

Acknowledgments We would like to thank Mike Shaw (University of Oxford) for assistance with scanning EM, David Studholme (University of Exeter) for assistance with bioinformatics, and Keith Gull (University of Oxford) for many helpful discussions. We are extremely grateful to Kidney Research UK and the Medical Research Council (Training Fellowship to RJS) and the Mason Medical Research Fellowship (for pump priming funding to RJS). We also acknowledge support from the Northern Counties Kidney Research Fund and Newcastle Hospitals Healthcare Charity (support for AMH), the Kids Kidney Research Fund (support for LE), the Beit Memorial Fellowships for Medical Research (to HRD), the EP Abraham Trust, and GlaxoSmithKline (Clinician Scientist Fellowship to JAS) for funding.

References

1. Maria BL, Hoang KB, Tusa RJ, Mancuso AA, Hamed LM, Quisling RG, Hove MT, Fennell EB, Booth-Jones M, Ringdahl DM, Yachnis AT, Creel G, Frerking B (1997) "Joubert syndrome" revisited: key ocular motor signs with magnetic resonance imaging correlation. J Child Neurol 12:423–430
2. Lambert SR, Kriss A, Gresty M, Benton S, Taylor D (1989) Joubert syndrome. Arch Ophthalmol 107:709–713
3. Sturm V, Leiba H, Menke MN, Valente EM, Poretti A, Landau K, Boltshauser E (2010) Ophthalmological findings in Joubert syndrome. Eye (Lond) 24:222–225
4. Utsch B, Sayer JA, Attanasio M, Pereira RR, Eccles M, Hennies HC, Otto EA, Hildebrandt F (2006) Identification of the first ahi1 gene mutations in nephronophthisis-associated Joubert syndrome. Pediatr Nephrol 21:32–35
5. Delous M, Baala L, Salomon R, Laclef C, Vierkotten J, Tory K, Golzio C, Lacoste T, Besse L, Ozilou C, Moutkine I, Hellman NE, Anselme I, Silbermann F, Vesque C, Gerhardt C, Rattenberry E, Wolf MT, Gubler MC, Martinovic J, Encha-Razavi F, Boddaert N, Gonzales M, Macher MA, Nivet H, Champion G, Bertheleme JP, Niaudet P, McDonald F, Hildebrandt F, Johnson CA, Vekemans M, Antignac C, Ruther U, Schneider-Maunoury S, Attie-Bitach T, Saunier S (2007) The ciliary gene rpgrip1l is mutated in cerebello-oculo-renal syndrome (Joubert syndrome type b) and Meckel syndrome. Nat Genet 39:875–881
6. Parisi MA, Doherty D, Chance PF, Glass IA (2007) Joubert syndrome (and related disorders) (omim 213300). Eur J Hum Genet 15:511–521
7. Brancati F, Dallapiccola B, Valente EM (2010) Joubert syndrome and related disorders. Orphanet J Rare Dis 5:20
8. Bielas SL, Silhavy JL, Brancati F, Kisseleva MV, Al-Gazali L, Sztriha L, Bayoumi RA, Zaki MS, Abdel-Aleem A, Rosti RO, Kayserili H, Swistun D, Scott LC, Bertini E, Boltshauser E, Fazzi E, Travaglini L, Field SJ, Gayral S, Jacoby M, Schurmans S, Dallapiccola B, Majerus PW, Valente EM, Gleeson JG (2009) Mutations in inpp5e, encoding inositol polyphosphate-5-phosphatase e, link phosphatidyl inositol signaling to the ciliopathies. Nat Genet 41:1032–1036
9. Edvardson S, Shaag A, Zenvirt S, Erlich Y, Hannon GJ, Shanske AL, Gomori JM, Ekstein J, Elpeleg O (2010) Joubert syndrome 2 (jbts2) in Ashkenazi Jews is associated with a tmem216 mutation. Am J Hum Genet 86:93–97
10. Ferland RJ, Eyaid W, Collura RV, Tully LD, Hill RS, Al-Nouri D, Al-Rumayyan A, Topcu M, Gascon G, Bodell A, Shugart YY, Ruvolo M, Walsh CA (2004) Abnormal cerebellar development and axonal decussation due to mutations in ahi1 in Joubert syndrome. Nat Genet 36:1008–1013
11. Parisi MA, Bennett CL, Eckert ML, Dobyns WB, Gleeson JG, Shaw DW, McDonald R, Eddy A, Chance PF, Glass IA (2004) The *nphp1* gene deletion associated with juvenile nephronophthisis is present in a subset of individuals with Joubert syndrome. Am J Hum Genet 75:82–91
12. Sayer JA, Otto EA, O'Toole JF, Nurnberg G, Kennedy MA, Becker C, Hennies HC, Helou J, Attanasio M, Fausett BV, Utsch B, Khanna H, Liu Y, Drummond I, Kawakami I, Kusakabe T, Tsuda M, Ma L, Lee H, Larson RG, Allen SJ, Wilkinson CJ, Nigg EA, Shou C, Lillo C, Williams DS, Hoppe B, Kemper MJ, Neuhaus T, Parisi MA, Glass IA, Petry M, Kispert A, Gloy J, Ganner A, Walz G, Zhu X, Goldman D, Nurnberg P, Swaroop A, Leroux MR, Hildebrandt F (2006) The centrosomal protein nephrocystin-6 is mutated in Joubert syndrome and activates transcription factor atf4. Nat Genet 38:674–681
13. Brancati F, Barrano G, Silhavy JL, Marsh SE, Travaglini L, Bielas SL, Amorini M, Zablocka D, Kayserili H, Al-Gazali L, Bertini E, Boltshauser E, D'Hooghe M, Fazzi E, Fenerci EY, Hennekam RC, Kiss A, Lees MM, Marco E, Phadke SR, Rigoli L, Romano S, Salpietro CD, Sherr EH, Signorini S, Stromme P, Stuart B, Sztriha L, Viskochil DH, Yuksel A, Dallapiccola B, Valente EM, Gleeson JG (2007) Cep290 mutations are frequently identified in the oculo-renal form of Joubert syndrome-related disorders. Am J Hum Genet 81:104–113

14. Valente EM, Silhavy JL, Brancati F, Barrano G, Krishnaswami SR, Castori M, Lancaster MA, Boltshauser E, Boccone L, Al-Gazali L, Fazzi E, Signorini S, Louie CM, Bellacchio E, Bertini E, Dallapiccola B, Gleeson JG (2006) Mutations in cep290, which encodes a centrosomal protein, cause pleiotropic forms of Joubert syndrome. Nat Genet 38:623–625
15. Smith UM, Consugar M, Tee LJ, McKee BM, Maina EN, Whelan S, Morgan NV, Goranson E, Gissen P, Lilliquist S, Aligianis IA, Ward CJ, Pasha S, Punyashthiti R, Malik Sharif S, Batman PA, Bennett CP, Woods CG, McKeown C, Bucourt M, Miller CA, Cox P, Algazali L, Trembath RC, Torres VE, Attie-Bitach T, Kelly DA, Maher ER, Gattone VH II, Harris PC, Johnson CA (2006) The transmembrane protein meckelin (mks3) is mutated in Meckel-Gruber syndrome and the wpk rat. Nat Genet 38:191–196
16. Baala L, Audollent S, Martinovic J, Ozilou C, Babron MC, Sivanandamoorthy S, Saunier S, Salomon R, Gonzales M, Rattenberry E, Esculpavit C, Toutain A, Moraine C, Parent P, Marcorelles P, Dauge MC, Roume J, Le Merrer M, Meiner V, Meir K, Menez F, Beaufrere AM, Francannet C, Tantau J, Sinico M, Dumez Y, MacDonald F, Munnich A, Lyonnet S, Gubler MC, Genin E, Johnson CA, Vekemans M, Encha-Razavi F, Attie-Bitach T (2007) Pleiotropic effects of cep290 (nphp6) mutations extend to Meckel syndrome. Am J Hum Genet 81:170–179
17. Cantagrel V, Silhavy JL, Bielas SL, Swistun D, Marsh SE, Bertrand JY, Audollent S, Attie-Bitach T, Holden KR, Dobyns WB, Traver D, Al-Gazali L, Ali BR, Lindner TH, Caspary T, Otto EA, Hildebrandt F, Glass IA, Logan CV, Johnson CA, Bennett C, Brancati F, Valente EM, Woods CG, Gleeson JG (2008) Mutations in the cilia gene arl13b lead to the classical form of Joubert syndrome. Am J Hum Genet 83:170–179
18. Gorden NT, Arts HH, Parisi MA, Coene KL, Letteboer SJ, van Beersum SE, Mans DA, Hikida A, Eckert M, Knutzen D, Alswaid AF, Ozyurek H, Dibooglu S, Otto EA, Liu Y, Davis EE, Hutter CM, Bammler TK, Farin FM, Dorschner M, Topcu M, Zackai EH, Rosenthal P, Owens KN, Katsanis N, Vincent JB, Hildebrandt F, Rubel EW, Raible DW, Knoers NV, Chance PF, Roepman R, Moens CB, Glass IA, Doherty D (2008) Cc2d2a is mutated in Joubert syndrome and interacts with the ciliopathy-associated basal body protein cep290. Am J Hum Genet 83:559–571
19. Coene KL, Roepman R, Doherty D, Afroze B, Kroes HY, Letteboer SJ, Ngu LH, Budny B, van Wijk E, Gorden NT, Azhimi M, Thauvin-Robinet C, Veltman JA, Boink M, Kleefstra T, Cremers FP, van Bokhoven H, de Brouwer AP (2009) Ofd1 is mutated in x-linked Joubert syndrome and interacts with lca5-encoded lebercilin. Am J Hum Genet 85:465–481
20. Hildebrandt F, Attanasio M, Otto E (2009) Nephronophthisis: disease mechanisms of a ciliopathy. J Am Soc Nephrol 20:23–35
21. Berbari NF, O'Connor AK, Haycraft CJ, Yoder BK (2009) The primary cilium as a complex signaling center. Curr Biol 19:R526–R535
22. Sang L, Miller JJ, Corbit KC, Giles RH, Brauer MJ, Otto EA, Baye LM, Wen X, Scales SJ, Kwong M, Huntzicker EG, Sfakianos MK, Sandoval W, Bazan JF, Kulkarni P, Garcia-Gonzalo FR, Seol AD, O'Toole JF, Held S, Reutter HM, Lane WS, Rafiq MA, Noor A, Ansar M, Devi AR, Sheffield VC, Slusarski DC, Vincent JB, Doherty DA, Hildebrandt F, Reiter JF, Jackson PK (2011) Mapping the nphp-jbts-mks protein network reveals ciliopathy disease genes and pathways. Cell 145:513–528
23. Dixon-Salazar T, Silhavy JL, Marsh SE, Louie CM, Scott LC, Gururaj A, Al-Gazali L, Al-Tawari AA, Kayserili H, Sztriha L, Gleeson JG (2004) Mutations in the *ahi1* gene, encoding jouberin, cause Joubert syndrome with cortical polymicrogyria. Am J Hum Genet 75:979–987
24. Valente EM, Brancati F, Silhavy JL, Castori M, Marsh SE, Barrano G, Bertini E, Boltshauser E, Zaki MS, Abdel-Aleem A, Abdel-Salam GM, Bellacchio E, Battini R, Cruse RP, Dobyns WB, Krishnamoorthy KS, Lagier-Tourenne C, Magee A, Pascual-Castroviejo I, Salpietro CD, Sarco D, Dallapiccola B, Gleeson JG (2006) Ahi1 gene mutations cause specific forms of Joubert syndrome-related disorders. Ann Neurol 59:527–534
25. Parisi MA, Doherty D, Eckert ML, Shaw DW, Ozyurek H, Aysun S, Giray O, Al Swaid A, Al Shahwan S, Dohayan N, Bakhsh E, Indridason OS, Dobyns WB, Bennett CL, Chance PF, Glass IA (2006) Ahi1 mutations cause both retinal dystrophy and renal cystic disease in Joubert syndrome. J Med Genet 43:334–339
26. Louie CM, Caridi G, Lopes VS, Brancati F, Kispert A, Lancaster MA, Schlossman AM, Otto EA, Leitges M, Grone HJ, Lopez I, Gudiseva HV, O'Toole JF, Vallespin E, Ayyagari R, Ayuso C, Cremers FP, den Hollander AI, Koenekoop RK, Dallapiccola B, Ghiggeri GM, Hildebrandt F, Valente EM, Williams DS, Gleeson JG (2010) Ahi1 is required for photoreceptor outer segment development and is a modifier for retinal degeneration in nephronophthisis. Nat Genet 42:175–180
27. Eley L, Gabrielides C, Adams M, Johnson CA, Hildebrandt F, Sayer JA (2008) Jouberin localizes to collecting ducts and interacts with nephrocystin-1. Kidney Int 74:1139–1149
28. Tory K, Lacoste T, Burglen L, Moriniere V, Boddaert N, Macher MA, Llanas B, Nivet H, Bensman A, Niaudet P, Antignac C, Salomon R, Saunier S (2007) High nphp1 and nphp6 mutation rate in patients with Joubert syndrome and nephronophthisis: Potential epistatic effect of nphp6 and ahi1 mutations in patients with nphp1 mutations. J Am Soc Nephrol 18:1566–1575
29. Doering JE, Kane K, Hsiao YC, Yao C, Shi B, Slowik AD, Dhagat B, Scott DD, Ault JG, Page-McCaw PS, Ferland RJ (2008) Species differences in the expression of ahi1, a protein implicated in the neurodevelopmental disorder Joubert syndrome, with preferential accumulation to stigmoid bodies. J Comp Neurol 511:238–256
30. Yen HJ, Tayeh MK, Mullins RF, Stone EM, Sheffield VC, Slusarski DC (2006) Bardet-Biedl syndrome genes are important in retrograde intracellular trafficking and Kupffer's vesicle cilia function. Hum Mol Genet 15:667–677
31. Essner JJ, Amack JD, Nyholm MK, Harris EB, Yost HJ (2005) Kupffer's vesicle is a ciliated organ of asymmetry in the zebrafish embryo that initiates left-right development of the brain, heart and gut. Development 132:1247–1260
32. Ahmad N, Long S, Rebagliati M (2004) A southpaw joins the roster: the role of the zebrafish nodal-related gene southpaw in cardiac lr asymmetry. Trends Cardiovasc Med 14:43–49
33. Altschul SF, Gish W, Miller W, Myers EW, Lipman DJ (1990) Basic local alignment search tool. J Mol Biol 215:403–410
34. Schultz J, Milpetz F, Bork P, Ponting CP (1998) Smart, a simple modular architecture research tool: identification of signaling domains. Proc Natl Acad Sci USA 95:5857–5864
35. Letunic I, Doerks T, Bork P (2009) Smart 6: recent updates and new developments. Nucleic Acids Res 37:D229–D232
36. Lupas A, Van Dyke M, Stock J (1991) Predicting coiled coils from protein sequences. Science 252:1162–1164
37. Kimmel CB, Ballard WW, Kimmel SR, Ullmann B, Schilling TF (1995) Stages of embryonic development of the zebrafish. Dev Dyn 203:253–310
38. Huang CJ, Tu CT, Hsiao CD, Hsieh FJ, Tsai HJ (2003) Germ-line transmission of a myocardium-specific gfp transgene reveals critical regulatory elements in the cardiac myosin light chain 2 promoter of zebrafish. Dev Dyn 228:30–40
39. Amack JD, Wang X, Yost HJ (2007) Two t-box genes play independent and cooperative roles to regulate morphogenesis of ciliated Kupffer's vesicle in zebrafish. Dev Biol 310:196–210
40. Thisse C, Thisse B (2008) High-resolution in situ hybridization to whole-mount zebrafish embryos. Nat Protoc 3:59–69
41. Hashimoto H, Rebagliati M, Ahmad N, Muraoka O, Kurokawa T, Hibi M, Suzuki T (2004) The cerberus/dan-family protein charon

is a negative regulator of nodal signaling during left-right patterning in zebrafish. Development 131:1741–1753
42. Krauss S, Concordet JP, Ingham PW (1993) A functionally conserved homolog of the drosophila segment polarity gene hh is expressed in tissues with polarizing activity in zebrafish embryos. Cell 75:1431–1444
43. Yelon D, Horne SA, Stainier DY (1999) Restricted expression of cardiac myosin genes reveals regulated aspects of heart tube assembly in zebrafish. Dev Biol 214:23–37
44. Malicki J, Neuhauss SC, Schier AF, Solnica-Krezel L, Stemple DL, Stainier DY, Abdelilah S, Zwartkruis F, Rangini Z, Driever W (1996) Mutations affecting development of the zebrafish retina. Development 123:263–273
45. Woods A, Sherwin T, Sasse R, MacRae TH, Baines AJ, Gull K (1989) Definition of individual components within the cytoskeleton of *Trypanosoma brucei* by a library of monoclonal antibodies. J Cell Sci 93(Pt 3):491–500
46. Dawe HR, Smith UM, Cullinane AR, Gerrelli D, Cox P, Badano JL, Blair-Reid S, Sriram N, Katsanis N, Attie-Bitach T, Afford SC, Copp AJ, Kelly DA, Gull K, Johnson CA (2007) The Meckel-Gruber syndrome proteins mks1 and meckelin interact and are required for primary cilium formation. Hum Mol Genet 16:173–186
47. Shi Z, Liang N, Xu W, Li K, Sheng G, Liu J, Xu A, Li XJ, Wu D (2009) Expression, purification, crystallization and preliminary x-ray crystallographic analysis of the sh3 domain of human ahi1. Acta Crystallogr Sect F Struct Biol Cryst Commun 65:361–363
48. Zhou W, Song P (2006) Molecular cloning of a novel gene zahi-1 and its expression analysis during zebrafish gametogenesis. Mol Biol Rep 33:111–116
49. Wang G, Cadwallader AB, Jang DS, Tsang M, Yost HJ, Amack JD (2011) The rho kinase rock2b establishes anteroposterior asymmetry of the ciliated Kupffer's vesicle in zebrafish. Development 138:45–54
50. Chen JN, van Eeden FJ, Warren KS, Chin A, Nusslein-Volhard C, Haffter P, Fishman MC (1997) Left-right pattern of cardiac bmp4 may drive asymmetry of the heart in zebrafish. Development 124:4373–4382
51. Chin AJ, Tsang M, Weinberg ES (2000) Heart and gut chiralities are controlled independently from initial heart position in the developing zebrafish. Dev Biol 227:403–421
52. Matter K, Balda MS (2003) Functional analysis of tight junctions. Methods 30:228–234
53. Zegers MM, O'Brien LE, Yu W, Datta A, Mostov KE (2003) Epithelial polarity and tubulogenesis in vitro. Trends Cell Biol 13:169–176
54. Li JB, Gerdes JM, Haycraft CJ, Fan Y, Teslovich TM, May-Simera H, Li H, Blacque OE, Li L, Leitch CC, Lewis RA, Green JS, Parfrey PS, Leroux MR, Davidson WS, Beales PL, Guay-Woodford LM, Yoder BK, Stormo GD, Katsanis N, Dutcher SK (2004) Comparative genomics identifies a flagellar and basal body proteome that includes the bbs5 human disease gene. Cell 117:541–552
55. Keller LC, Romijn EP, Zamora I, Yates JR III, Marshall WF (2005) Proteomic analysis of isolated chlamydomonas centrioles reveals orthologs of ciliary-disease genes. Curr Biol 15:1090–1098
56. Liu Q, Tan G, Levenkova N, Li T, Pugh EN Jr, Rux JJ, Speicher DW, Pierce EA (2007) The proteome of the mouse photoreceptor sensory cilium complex. Mol Cell Proteomics 6:1299–1317
57. Hsiao YC, Tong ZJ, Westfall JE, Ault JG, Page-McCaw PS, Ferland RJ (2009) Ahi1, whose human ortholog is mutated in Joubert syndrome, is required for rab8a localization, ciliogenesis and vesicle trafficking. Hum Mol Genet 18:3926–3941
58. Avidor-Reiss T, Maer AM, Koundakjian E, Polyanovsky A, Keil T, Subramaniam S, Zuker CS (2004) Decoding cilia function: defining specialized genes required for compartmentalized cilia biogenesis. Cell 117:527–539
59. Broadhead R, Dawe HR, Farr H, Griffiths S, Hart SR, Portman N, Shaw MK, Ginger ML, Gaskell SJ, McKean PG, Gull K (2006) Flagellar motility is required for the viability of the bloodstream trypanosome. Nature 440:224–227
60. Sieburth JM, Johnson PW, Hargreaves PE (1988) Ultrastructure and ecology of *Aureococcus anophagefferens* gen et sp. nov. (Chrysophyceae): the dominant picoplankter during a bloom in Narragansett Bay, Rhode Island, summer 1985. J Phycol 24:416–425
61. Blanc G, Duncan G, Agarkova I, Borodovsky M, Gurnon J, Kuo A, Lindquist E, Lucas S, Pangilinan J, Polle J, Salamov A, Terry A, Yamada T, Dunigan DD, Grigoriev IV, Claverie JM, Van Etten JL (2010) The *Chlorella variabilis* nc64a genome reveals adaptation to photosymbiosis, coevolution with viruses, and cryptic sex. Plant Cell 22:2943–2955
62. Hodges ME, Scheumann N, Wickstead B, Langdale JA, Gull K (2010) Reconstructing the evolutionary history of the centriole from protein components. J Cell Sci 123:1407–1413
63. Elias M, Archibald JM (2009) The rjl family of small GTPases is an ancient eukaryotic invention probably functionally associated with the flagellar apparatus. Gene 442:63–72
64. Woodland HR, Fry AM (2008) Pix proteins and the evolution of centrioles. PLoS One 3:e3778
65. Jensen KG, Moestrup O, Schmid AMM (2003) Ultrastructure of the male gametes from two centric diatoms, *Chaetoceros laciniosus* and *Coscinodiscus wailesii* (Bacillariophyceae). Phycologia 42:98–105
66. Sorokin S (1962) Centrioles and the formation of rudimentary cilia by fibroblasts and smooth muscle cells. J Cell Biol 15:363–377
67. Molla-Herman A, Ghossoub R, Blisnick T, Meunier A, Serres C, Silbermann F, Emmerson C, Romeo K, Bourdoncle P, Schmitt A, Saunier S, Spassky N, Bastin P, Benmerah A (2010) The ciliary pocket: an endocytic membrane domain at the base of primary and motile cilia. J Cell Sci 123:1785–1795
68. Baldari CT, Rosenbaum J (2010) Intraflagellar transport: it's not just for cilia anymore. Curr Opin Cell Biol 22:75–80
69. Tsiokas L, Kim S, Ong EC (2007) Cell biology of polycystin-2. Cell Signal 19:444–453
70. Yachnis AT, Rorke LB (1999) Neuropathology of Joubert syndrome. J Child Neurol 14:655–659 discussion 669-672
71. Yachnis AT, Rorke LB (1999) Cerebellar and brainstem development: an overview in relation to Joubert syndrome. J Child Neurol 14:570–573
72. Sheng G, Xu X, Lin YF, Wang CE, Rong J, Cheng D, Peng J, Jiang X, Li SH, Li XJ (2008) Huntingtin-associated protein 1 interacts with ahi1 to regulate cerebellar and brainstem development in mice. J Clin Invest 118:2785–2795
73. Wingert RA, Davidson AJ (2008) The zebrafish pronephros: a model to study nephron segmentation. Kidney Int 73:1120–1127
74. Simms RJ, Eley L, Sayer JA (2009) Nephronophthisis. Eur J Hum Genet 17:406–416
75. Beales PL, Bland E, Tobin JL, Bacchelli C, Tuysuz B, Hill J, Rix S, Pearson CG, Kai M, Hartley J, Johnson C, Irving M, Elcioglu N, Winey M, Tada M, Scambler PJ (2007) Ift80, which encodes a conserved intraflagellar transport protein, is mutated in jeune asphyxiating thoracic dystrophy. Nat Genet 39:727–729
76. Duldulao NA, Lee S, Sun Z (2009) Cilia localization is essential for in vivo functions of the Joubert syndrome protein arl13b/scorpion. Development 136:4033–4042
77. Kishimoto N, Cao Y, Park A, Sun Z (2008) Cystic kidney gene seahorse regulates cilia-mediated processes and wnt pathways. Dev Cell 14:954–961

78. Serluca FC, Xu B, Okabe N, Baker K, Lin SY, Sullivan-Brown J, Konieczkowski DJ, Jaffe KM, Bradner JM, Fishman MC, Burdine RD (2009) Mutations in zebrafish leucine-rich repeat-containing six-like affect cilia motility and result in pronephric cysts, but have variable effects on left-right patterning. Development 136:1621–1631
79. Sullivan-Brown J, Schottenfeld J, Okabe N, Hostetter CL, Serluca FC, Thiberge SY, Burdine RD (2008) Zebrafish mutations affecting cilia motility share similar cystic phenotypes and suggest a mechanism of cyst formation that differs from pkd2 morphants. Dev Biol 314:261–275
80. Ferrante MI, Romio L, Castro S, Collins JE, Goulding DA, Stemple DL, Woolf AS, Wilson SW (2009) Convergent extension movements and ciliary function are mediated by ofd1, a zebrafish orthologue of the human oral-facial-digital type 1 syndrome gene. Hum Mol Genet 18:289–303
81. Otto EA, Schermer B, Obara T, O'Toole JF, Hiller KS, Mueller AM, Ruf RG, Hoefele J, Beekmann F, Landau D, Foreman JW, Goodship JA, Strachan T, Kispert A, Wolf MT, Gagnadoux MF, Nivet H, Antignac C, Walz G, Drummond IA, Benzing T, Hildebrandt F (2003) Mutations in invs encoding inversin cause nephronophthisis type 2, linking renal cystic disease to the function of primary cilia and left-right axis determination. Nat Genet 34:413–420
82. Bergmann C, Fliegauf M, Bruchle NO, Frank V, Olbrich H, Kirschner J, Schermer B, Schmedding I, Kispert A, Kranzlin B, Nurnberg G, Becker C, Grimm T, Girschick G, Lynch SA, Kelehan P, Senderek J, Neuhaus TJ, Stallmach T, Zentgraf H, Nurnberg P, Gretz N, Lo C, Lienkamp S, Schafer T, Walz G, Benzing T, Zerres K, Omran H (2008) Loss of nephrocystin-3 function can cause embryonic lethality, Meckel-Gruber-like syndrome, situs inversus, and renal-hepatic-pancreatic dysplasia. Am J Hum Genet 82:959–970